JCB Journal of Cell Biology

ARTICLE

Structural insight into microtubule stabilization and kinesin inhibition by Tau family MAPs

Hideki Shigematsu[1,2*], Tsuyoshi Imasaki[3,4*], Chihiro Doki[5], Takuya Sumi[3], Mari Aoki[1,6], Tomomi Uchikubo-Kamo[1,6], Ayako Sakamoto[1,6], Kiyotaka Tokuraku[5], Mikako Shirouzu[1,6], and Ryo Nitta[1,3]

The Tau family microtubule-associated proteins (MAPs) promote microtubule stabilization and regulate microtubule-based motility. They share the C-terminal microtubule-binding domain, which includes three to five tubulin-binding repeats. Different numbers of repeats formed by alternative splicing have distinct effects on the activities of these proteins, and the distribution of these variants regulates fundamental physiological phenomena in cells. In this study, using cryo-EM, we visualized the MAP4 microtubule complex with the molecular motor kinesin-1. MAP4 bound to the C-terminal domains of tubulins along the protofilaments stabilizes the longitudinal contacts of the microtubule. The strongest bond of MAP4 was found around the intertubulin–dimer interface such that MAP4 coexists on the microtubule with kinesin-1 bound to the intratubulin–dimer interface as well. MAP4, consisting of five repeats, further folds and accumulates above the intertubulin–dimer interface, interfering with kinesin-1 movement. Therefore, these cryo-EM studies reveal new insight into the structural basis of microtubule stabilization and inhibition of kinesin motility by the Tau family MAPs.

Introduction

The tau family of microtubule-associated proteins (MAPs), including Tau, MAP2, and MAP4, promote microtubule assembly and stability in vertebrates. Tau and MAP2 are abundant in the axons and dendrites of neurons, respectively, and they contribute to neuritogenesis, whereas MAP4 is distributed in glial cells and many other nonneuronal cells including muscle tissues (Drewes et al., 1998). They all share a similar architecture composed of a conserved C-terminal microtubule-binding domain and an N-terminal projection domain that is distinct in each MAP (Fig. 1 A; Dehmelt and Halpain, 2005). The former consists of tubulin-binding motifs of ∼18 residues known as assembly promoting (AP) sequences. These are arrayed in three to four imperfect tandem repeats in Tau and MAP2 and in three to five repeats in MAP4, separated by flexible linkers. Different numbers of repeats are generated by alternative splicing of a single gene, thereby producing several isoforms that are observed in all tau family MAPs (Ennulat et al., 1989; Joly et al., 1989; Aizawa et al., 1990).

There have been several studies that described different effects produced by the distinct isoforms of MAPs on microtubule dynamics or on the motility of microtubule-based motor. Isoforms of Tau containing three (3R) or four (4R) tubulin-binding repeats have distinct effects on microtubule dynamics; 4R-tau protects microtubules from depolymerization much more robustly than 3R-tau (Panda et al., 2003). Consistently, the increasing ratio of 4R-tau to 3R-tau is considered to lead to frontotemporal dementia (FTDP-17; Hardy et al., 1998; Spillantini and Goedert, 1998). Moreover, the splicing variants MAP2a, MAP2b, and MAP2c are differentially expressed during the progression of neuronal development, suggesting that they play distinct roles (Gamblin et al., 1996). For MAP4, a different number of repeat sequences from 3R to 5R alters the microtubule bundling activity in vitro (Tokuraku et al., 2003). More recently, differential expressions of MAP4 isoforms in skeletal muscle cells were reported (Mogessie et al., 2015). The 3R-MAP4 aligns dynamic microtubules into antiparallel bundles to organize the paraxial microtubule array required for muscle cell differentiation, whereas 5R-MAP4 does not. 3R-MAP4 is expressed during the myogenesis of skeletal muscles, whereas 5R-MAP4 is majorly expressed in mature skeletal muscle cells or cardiomyocytes. These studies collectively indicated that the splice variants with different numbers of tubulin-binding repeats are temporospatially regulated to achieve their distinct roles.

Tau family MAPs also reportedly inhibit kinesin- and dynein-dependent transport along microtubules (Hagiwara et

[1]RIKEN Center for Life Science Technologies, Yokohama, Japan; [2]RIKEN SPring-8 Center, Hyogo, Japan; [3]Division of Structural Medicine and Anatomy, Department of Physiology and Cell Biology, Kobe University Graduate School of Medicine, Kobe, Japan; [4]Precursory Research for Embryonic Science and Technology (PRESTO), Japan Science and Technology Agency, Saitama, Japan; [5]Division of Applied Science and Engineering, Course of Biosystem, Graduate School of Muroran Institute of Technology, Muroran, Japan; [6]RIKEN Center for Biosystems Dynamics Research, Yokohama, Japan.

*H. Shigematsu and T. Imasaki contributed equally to this paper; Correspondence to Ryo Nitta: ryonitta@med.kobe-u.ac.jp.

© 2018 Shigematsu et al. This article is distributed under the terms of an Attribution–Noncommercial–Share Alike–No Mirror Sites license for the first six months after the publication date (see http://www.rupress.org/terms/). After six months it is available under a Creative Commons License (Attribution–Noncommercial–Share Alike 4.0 International license, as described at https://creativecommons.org/licenses/by-nc-sa/4.0/).

al., 1994; Ebneth et al., 1998; Trinczek et al., 1999; Seitz et al., 2002; Tokuraku et al., 2007). This inhibition is predominantly caused by a direct competition between MAPs and kinesins for microtubule binding. The attachment frequency of motors is reduced in the presence of MAPs, although kinesin moves normally once it attaches to the microtubule (Trinczek et al., 1999). However, in addition to the direct competition for microtubule binding, 5R-MAP4 completely impedes the movement of kinesin even after the kinesin attaches to the microtubule (Tokuraku et al., 2007). Considering that the 5R isoform has been found only in nonneuronal MAP4 and not in neuronal Tau or MAP2, a distinct regulation for organelle transport might be necessary in both neurons and nonneuronal cells.

Because of the physiological importance of the Tau family MAPs, numerous studies have focused on their biochemical properties and/or structures. However, natively unfolded molecules exist in these proteins (Schweers et al., 1994), which preclude detailed structural analyses. Quick-freeze deep-etch EM elucidated that Tau and MAP2 bind to the outer surface of the microtubule lattice and that the length of the projection domain can regulate microtubule spacing (Hirokawa et al., 1988; Chen et al., 1992). Cross-linking studies identified the potential binding regions on α- or β-tubulins as the C-terminal helices H11 and H12 and the C-terminal E-hook (Chau et al., 1998). Subsequent cryo-EM studies consistently indicated that the tubulin-binding repeats of Tau or MAP2 bind longitudinally along the outer ridge of the microtubule protofilament (Al-Bassam et al., 2002; Santarella et al., 2004). However, another cryo-EM analysis also suggested that Tau binds to the inner microtubule surface adjacent to the paclitaxel-binding site (Kar et al., 2003). Thus, because of the limited resolution of cryo-EM studies, the structural property of Tau/MAP2/MAP4 that get attached to the microtubules remains incompletely understood.

Here we present a cryo-EM reconstruction of the MAP4–kinesin-1–microtubule complex. We used two types of MAP4 constructs, 4R-MAP4 (termed as PA_4T; Tokuraku et al., 2007) and 5R-MAP4 (termed as PA_5T; Tokuraku et al., 2007) because their biochemical properties, the effects for the microtubule stability, and the microtubule-based kinesin-1 motility were well studied (Fig. 1 A; Tokuraku et al., 2003, 2007). Either 4R-MAP4 or 5R-MAP4 coexists with kinesin-1 on the microtubule; MAP4 exists around the intertubulin–dimer interface of the microtubule, whereas kinesin-1 is located around the intratubulin–dimer interface of the microtubule. 5R-MAP4 is much more stabilized on the microtubule than 4R-MAP4, probably owing to the interaction of kinesin-1, which accumulates far above the intertubulin–dimer groove. Thus, we provide the first structural evidence for microtubule stabilization by MAP4 as well as the inhibitory effect of MAP4 for kinesin-dependent transport along the microtubule.

Results

MAP4 and kinesin-1 can be simultaneously bound to the microtubules

We first examined the microtubule-binding ability of both 4R-MAP4 and 5R-MAP4 (Fig. 1 A) by performing microtubule copelleting assays (Fig. 1 B). In comparison with tubulin alone, a lesser number of tubulins were found in the supernatant fractions, indicating that more tubulins had polymerized into microtubules in the presence of 4R-MAP4 or 5R-MAP4 even at a molar concentration one-third of the tubulin concentration. The molar ratio between MAP4 and tubulin monomer in the pellet fractions is ∼1:4–5 at a saturated concentration of MAP4 (Fig. 1 C). No significant difference was found in the tubulin binding ratio between 4R-MAP4 and 5R-MAP4 (unpaired *t* test; P = 0.436). If one tubulin-binding repeat in the AP sequence of MAP4 is bound to one tubulin monomer as previously predicted (Chau et al., 1998; Al-Bassam et al., 2002), four to five tubulin-binding repeats would be required to achieve this stoichiometry. In this case, most of the tubulin-binding repeats of 4R-MAP4 or 5R-MAP4 should contribute toward microtubule binding.

Next, we investigated the microtubule-binding properties of MAP4 and kinesin-1. We tested whether kinesin-1 and MAP4 affect the binding of each other to the microtubule. The 5-µM microtubule surface was first saturated by 20 µM kinesin-1, and 3.2, 6.4, 9.6, 12.8, and 16 µM 4R-MAP4 or 5R-MAP4 was subsequently added. As a control, MAP4 binding in the absence of kinesin-1 was also examined. Consequently, kinesin-1 did not interfere with the binding of 4R-MAP4 or 5R-MAP4 to the microtubule, and MAP4 binding did not affect kinesin-1 binding to the microtubule (Fig. 1, D and E). We also performed the opposite experiment. The 5-µM microtubule surface was first saturated by 10 µM 4R-MAP4 or 5R-MAP4, and 4, 8, 12, 16, or 20 µM kinesin-1 was subsequently added. As a control, kinesin-1 binding in the absence of MAP4 was examined. Consequently, neither 4R-MAP4 nor 5R-MAP4 blocked kinesin-1 from binding to the microtubule, and kinesin-1 binding did not cause MAP4 to dissociate from the microtubule (Fig. 1, F and G). Therefore, MAP4 can coexist with kinesin-1 along the microtubule, and the number of MAP4 or kinesin-1 molecules bound to the microtubule is not affected by the saturating conditions of the other molecule. In other words, the binding stoichiometry between MAP4 and tubulin or between kinesin-1 and tubulin did not change in the presence of kinesin-1 or MAP4, respectively. However, it should be noted that the possibility of competition between MAP4 and kinesin-1 upon attachment to the microtubule should not be excluded because we observed the binding of MAP4 and/or kinesin-1 to the microtubule in the equilibrium state. One possible explanation is that the binding sites of MAP4 and kinesin-1 in the microtubule are at different locations or that MAP4 has two or more binding sites, at least one of which is different from the kinesin-1 binding site.

Cryo-EM reconstruction of the MAP4–kinesin-1–microtubule complex

Microtubule-binding assays indicated that MAP4 and kinesin-1 simultaneously attached to the microtubules. Thus, we performed cryo-EM analysis of the 4R-MAP4–kinesin-1–microtubule and 5R-MAP4–kinesin-1–microtubule complexes. Because GDP–microtubule combined with paclitaxel (taxol–microtubule) was used in our previous study of kinesin-1 inhibition by 5R-MAP4 (Tokuraku et al., 2007), the taxol–microtubule was also used in the cryo-EM reconstruction procedure. Fast Fourier transform of the micrograph showed the layer lines at 4 and 8 nm derived from

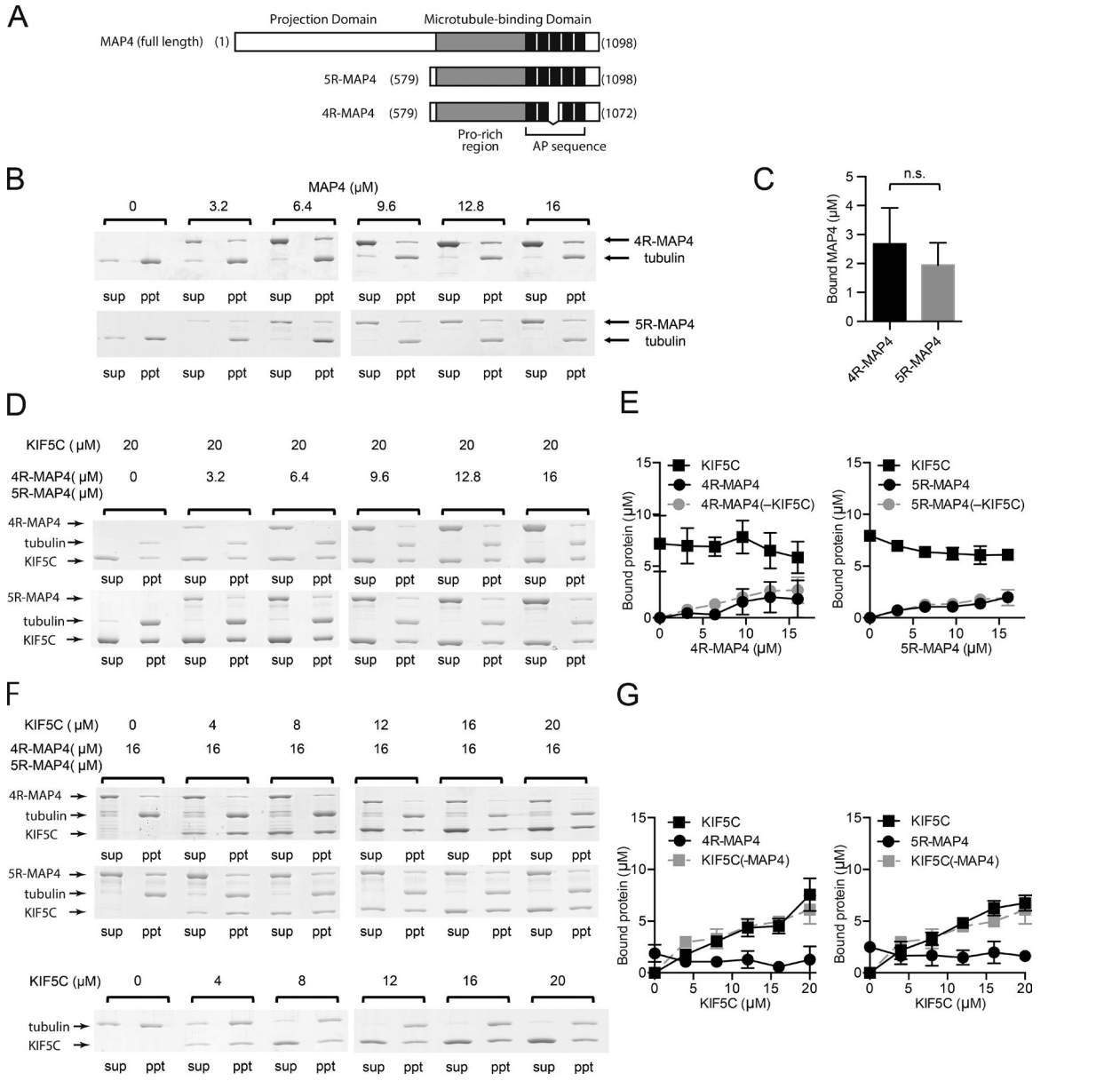

Figure 1. **MAP4 and kinesin-1 can be simultaneously bound to the microtubules. (A)** Primary structure of MAP4 and its microtubule-binding fragments 5R-MAP4 and 4R-MAP4. **(B–G)** Microtubule cosedimentation assays. All experiments were performed three independent times, and the concentrations of bound protein were calculated from each SDS-PAGE gel. Error bars in graphs represent SD (n = 3). **(B)** Typical SDS-PAGE gels of microtubule-binding assays of 4R- or 5R-MAP4 without kinesin-1. **(C)** Concentrations of bound MAP4 fragments when 16 μM 4R- or 5R-MAP4 was incubated with microtubules (in the absence of kinesin-1). There was no significant difference between the bound 4R- and 5R-MAP4. **(D)** Typical results for binding of 4R- or 5R-MAP4 to microtubules in the presence of 20 μM kinesin-1. **(E)** The concentrations of bound 4R- or 5R-MAP4 and kinesin-1 in the presence of 20 μM kinesin-1. The concentrations of bound 4R- or 5R-MAP4 in the absence of kinesin-1 are also shown. **(F)** Typical results of microtubule-binding assays of kinesin-1 with 16 μM 4R- or 5R-MAP4. Sup, supernatant; ppt, precipitate. **(G)** The concentrations of bound kinesin-1 and 4R- or 5R-MAP4. The concentrations of bound kinesin-1 in the absence of MAP4 are also shown.

one tubulin–monomer repeat and one tubulin–dimer repeat (Fig. S1 A). Considering that the micrograph of MAP4–microtubule complex in the absence of kinesin-1 revealed a layer line only at 4 nm (Fig. S1 B), MAP4 would not be bound to the microtubule at periodic intervals according to the three to five tubulin monomers (12, 16, and 20 nm); rather, each tubulin binding repeat in MAP4 would recognize each tubulin–monomer.

The cryo-EM reconstructions of the 4R-MAP4–kinesin-1–microtubule and the 5R-MAP4–kinesin-1–microtubule were performed at an overall resolution of ∼7 Å; the average resolutions in the tubulin region were <5 Å (Fig. 2; Fig. S1, C and D; and Fig. S2, C, D, G, and H). The lower resolution of surface densities corresponding with kinesin-1 and MAP4 in our cryo-EM reconstruction could be due to their flexibility and/or substoichiometric binding (Fig. S2, D and H). In this complex, kinesin-1 was in the ATP state, mimicked by the ATP analogue adenylyl-imidodiphosphate (AMP-PNP). The conformation of kinesin-1 and the microtubule in both reconstructions are quite similar to the previously resolved cryo-EM structure

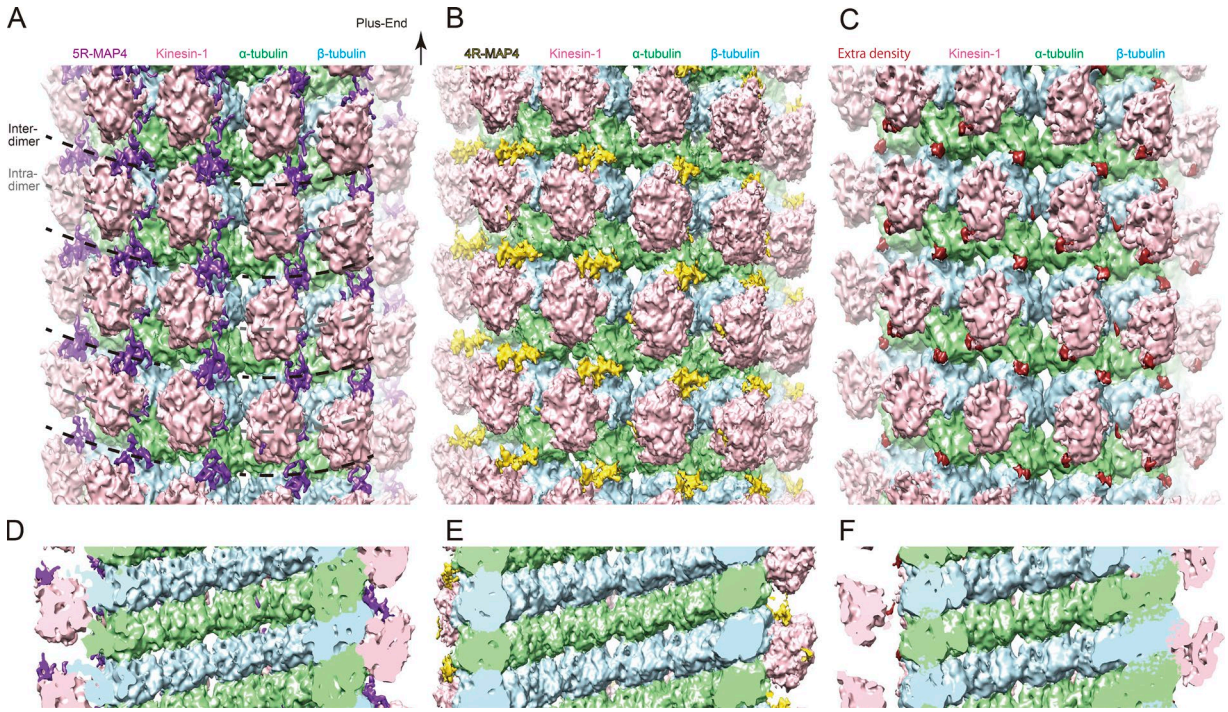

Figure 2. **Cryo-EM reconstructions of MAP4–kinesin-1–microtubule complex. (A and D)** Cryo-EM reconstruction of 5R-MAP4–kinesin-1–microtubule complex. Green, α-tubulin; light blue, β-tubulin; pink, kinesin-1; purple, residual densities (5R-MAP4). **(B and E)** Cryo-EM reconstruction of 4R-MAP4–kinesin-1–microtubule complex. Yellow, residual densities (4R-MAP4). **(C and F)** Cryo-EM reconstruction of kinesin-1–microtubule complex. Red, residual densities. **(A–C)** Cryo-EM reconstructions observed from the outer surface of microtubules. **(D–F)** Cryo-EM reconstructions observed from the inside of microtubules.

of the kinesin-1–microtubule complex (Atherton et al., 2014). The atomic models of kinesin-1 and the α-, β-tubulin–dimer (PDB ID: 4UY0) were well fitted with our cryo-EM densities (Fig. S2, A, B, E, and F). The α-, β-tubulin–dimer conformation is essentially the same in both 4R-MAP4 and 5R-MAP4 complexes.

After rigid body fittings of atomic models of kinesin-1 and the tubulin monomer, the cryo-EM maps were segmented based on a cutoff distance of 5 Å from the fitted atomic models using UCSF Chimera (Pettersen et al., 2004). The 5R-MAP4–kinesin-1–microtubule (Fig. 2 A) and 4R-MAP4–kinesin-1–microtubule (Fig. 2 B) complexes are compared with the kinesin-1–microtubule complex without MAP4 (Fig. 2 C). They were divided into four segments, the kinesin-1 segment (pink in Fig. 2, A–C), α-tubulin segment (green in Fig. 2, A–C), β-tubulin segment (light blue in Fig. 2, A–C), and the remaining segment (purple, yellow, or red in Fig. 2, A–C). Consequently, more densities were found in the remaining segments of the 5R-MAP4 complex than in that of the 4R-MAP4 complex (Figs. 2, A and B; and Fig. S3, A–C). Considering that the least remaining segments were found in the kinesin-1–microtubule complex without MAP4, most of the densities found in the 5R-MAP4–kinesin-1–microtubule complex and 4R-MAP4–kinesin-1–microtubule complex are supposed to be derived from the MAP4 structure. Indeed, these densities were also not observed in the previously reported cryo-EM reconstruction of kinesin-1–taxol–microtubule complex without MAP4 (EMD-2770; Atherton et al., 2014), suggesting that the presence of MAP4 contributes to them. The C-terminal tail of the α- and β-tubulins (E-hook) may also be stabilized by MAP4 and thus possibly contribute to the residual density.

The remaining segments appeared to be much smaller than expected from the molecular weight of MAP4 moiety (4R-MAP4, 50.0 kD; 5R-MAP4, 52.7 kD), possibly because of the flexible nature of MAP4. The densities were concentrated on the right-hand side of the protofilament ridge around the intertubulin–dimer interface in both 4R-MAP4 and 5R-MAP4 complexes (purple in Fig. 2 A and yellow in Fig. 2 B). Although kinesin-1 was mainly bound to the left-hand side of the protofilament ridge, MAP4 densities seem to be interrupted by the kinesin-1 densities. In addition, almost no extra density was observed on the lateral contact or inside of the microtubule, suggesting that there is no stable region of MAP4 located on the lateral side or inside of the microtubule (Fig. 2, D–F).

Structural detail of MAP4–kinesin-1–microtubule binding

We focus on the MAP4 densities in the MAP4–kinesin-1–microtubule complex to investigate further the remaining densities. The most prominent density was found around the intertubulin–dimer groove, which serves as the polymerization interface (Fig. 3, A and B). MAP4 is bound to both α- and β-tubulin to bridge the interface, thus stabilizing the polymerized microtubules. The density of 4R-MAP4 is found only around this site (Fig. 3 B). On the other hand, 5R-MAP4 extends toward the plus- and minus-end sides along the C-terminal helices (H11 and H12) of tubulins (Fig. 3, A and C). However, it seems to be interrupted around the intratubulin–dimer groove where kinesin-1 occupies the microtubule surface.

To further investigate the structural detail of 5R-MAP4 binding, the recently reported atomic model of Tau was superim-

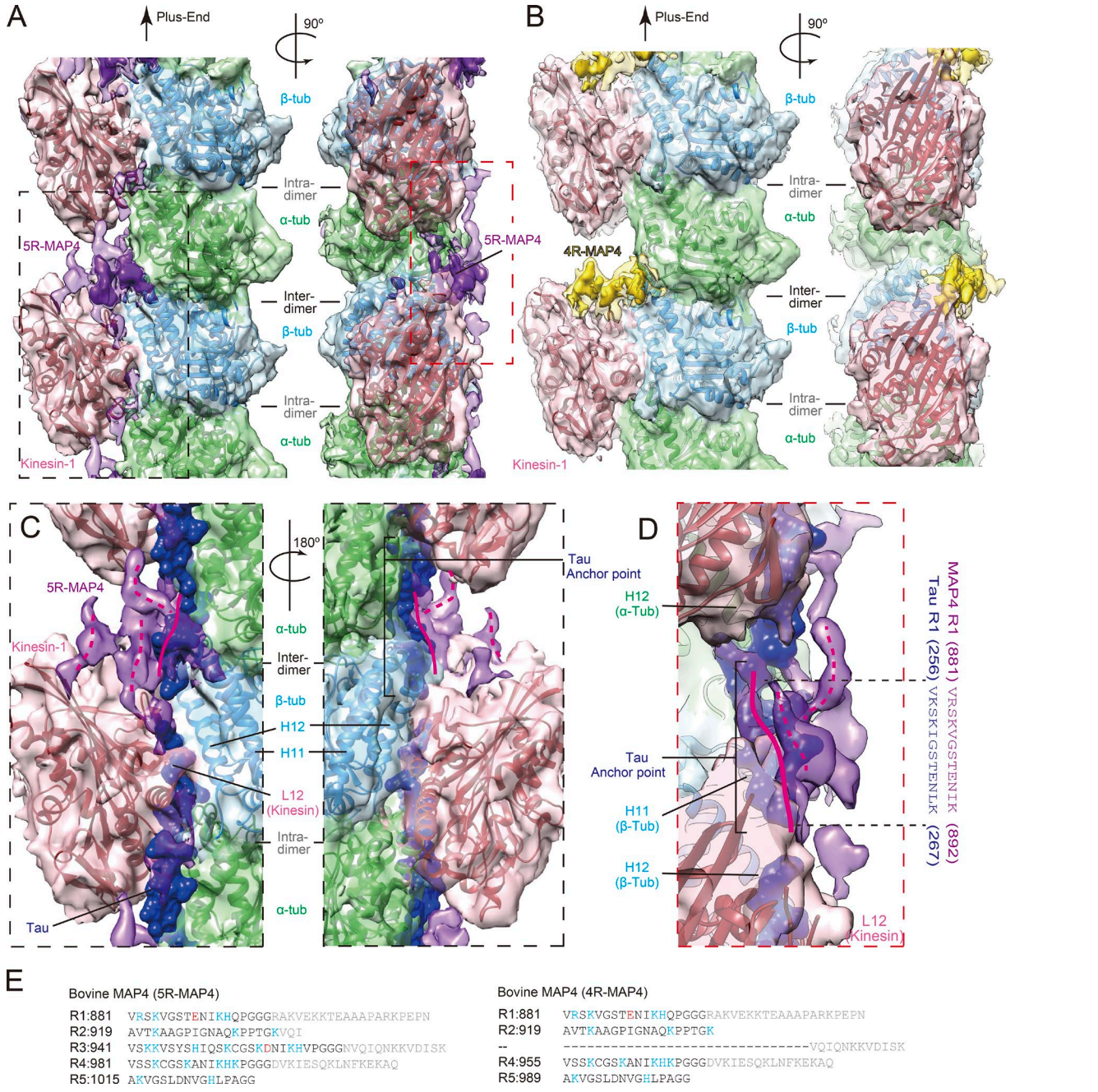

Figure 3. **Structural detail of MAP4–kinesin-1–microtubule binding. (A)** Cryo-EM reconstruction of 5R-MAP4–kinesin-1–microtubule complex seen from the right side of the protofilament (left) and from the surface (right). Green, α-tubulin; light blue, β-tubulin; pink, kinesin-1; purple, 5R-MAP4. Higher threshold density for MAP4 is shown in opaque. **(B)** Cryo-EM reconstruction of 4R-MAP4–kinesin-1–microtubule complex. Green, α-tubulin; light blue, β-tubulin; pink, kinesin-1; yellow, 4R-MAP4. Higher threshold density for MAP4 is shown in opaque. **(C)** Magnified view of black dotted rectangle in A shown with Tau (blue; PDB ID: 6CVN). A 180°-rotated view is also presented. **(D)** Magnified view of red dotted rectangle in A shown with Tau. The anchor point sequences of Tau and corresponding sequence of MAP4 are also presented. **(E)** Amino acid sequences of the tubulin-binding repeat of bovine 5R-MAP4 and 4R-MAP4.

posed on our 5R-MAP4–kinesin-1–microtubule complex (PDB ID: 6CVN; Kellogg et al., 2018). Consequently, a part of the MAP4 density, which runs along the C-terminal helices (H11 and H12) of α- and β-tubulins around the interdimer groove, overlaps with the repeat sequence of Tau structure from amino acid Val 256 to Lys267 (solid magenta lines in Fig. 3, C and D). In reference to the Tau structure, the length of the overlapping region might be equivalent to the length of one tubulin-binding repeat sequence, namely the "anchor point" (Kellogg et al., 2018). It suggests that MAP4 would be bound to the C-terminal helices of the microtubule through one tubulin-binding repeat, similar to the Tau–microtubule interaction.

However, overlap was found between the Tau structure and kinesin-1 around the intradimer groove, suggesting that 5R-MAP4 in the presence of kinesin-1 could not take a similar elongated structure as Tau (Fig. 3, C and D). In our reconstruction,

5R-MAP4 further extends upward or rightward to the space surrounded by β-tubulin, α-tubulin, and two neighboring kinesin-1s, running along the microtubule axis (dotted magenta lines in Fig. 3, C and D). Thus, one tubulin-binding repeat should bind directly to C-terminal helices of the microtubule, and the other repeats connected by the conserved PGGG flexible sequence or/and the N-terminal proline-rich region may fold back upward or rightward to occupy the space between two neighboring kinesin-1 molecules along the protofilament (Fig. 3, C–E).

At the intratubulin–dimer interface, lower density was found, possibly to the L12 loop of kinesin-1 occupying this space (Fig. 3, A, C, and D). In fact, the L12 loop is rich in basic residues that repel the tubulin-binding repeat of MAP4, which is also rich in basic residues. The suspected competition for microtubule attachment between Tau family MAPs and kinesin-1 might be occurring at this site (Hagiwara et al., 1994; Ebneth et al., 1998; Trinczek et al., 1999; Seitz et al., 2002; Tokuraku et al., 2007).

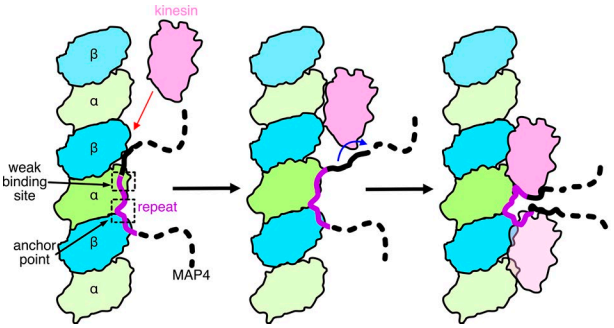

Figure 4. **Structural model of microtubule binding of MAP4 and kinesin inhibition by MAP4.** MAP4 is bound to the microtubule through the anchor point around the interdimer interface and through the weak binding site around the intradimer interface. Kinesin-1 competes against MAP4 for the weak binding site and finally eliminates MAP4 from the weak binding site. MAP4 is still anchored at the anchor point, and the rest of the regions may fold and accumulate above the interdimer interface.

Discussion

In this report, we visualized the cryo-EM structure of Tau family MAPs 4R- and 5R-MAP4, forming a complex with kinesin-1 and microtubules. We also successfully illustrated the structural difference between 4R-MAP4 and 5R-MAP4 bound to the microtubule. These cryo-EM reconstructions not only provide the structural basis for microtubule stabilization by Tau family MAPs, but they also provide the structural mechanism for the inhibition of kinesin-dependent transport by Tau family MAPs.

Tau family MAPs are intrinsically disordered proteins, so they do not take a uniform shape in solution. Thus, it is challenging to visualize their structure using x-ray crystallography or cryo-EM. Tau is known to form filamentous aggregates called neurofibrillary tangles whose structure were recently reported by high-resolution cryo-EM study without microtubules (Fitzpatrick et al., 2017). The low-resolution cryo-EM studies of the MAP–microtubule complex revealed the probable MAP-binding site on the microtubule (Al-Bassam et al., 2002; Santarella et al., 2004). More recently, near-atomic-resolution structure of Tau using a synthetic Tau construct was confirmed in a low-resolution cryo-EM study. Kellogg et al. (2018) reported that the conserved tubulin-binding repeats within tau adopt extended structures along the surface ridge of the protofilament. Tau–microtubule bonds were the strongest around the intertubulin–dimer groove, namely the anchor point, which was also conserved in the MAP4–kinesin-1–microtubule complex described in our study (Fig. 3, C and D; and Fig. 4). MAP4 bridges α- and β-tubulins at the anchor point, thereby stabilizing the longitudinal contacts of the microtubule.

Tau family MAPs are known to inhibit the microtubule-based kinesin motility (Hagiwara et al., 1994; Ebneth et al., 1998; Trinczek et al., 1999; Seitz et al., 2002; Tokuraku et al., 2007). As described above, MAP4 with three or four tubulin-binding repeats competes for microtubule-binding with kinesin-1. MAP4 with five repeats further stops kinesin-1 motility even after kinesin-1 is already bound to the microtubule (Tokuraku et al., 2007). From the structural study presented here, MAP4 in the presence of kinesin-1 mainly binds to the anchor point around the intertubulin–dimer interface, whereas a considerably lower MAP4 density was found around the intratubulin–dimer interface to which kinesin-1 binds (Fig. 3, A and B). Considering that Tau is weakly bound to the microtubule around the intratubulin–dimer interface (weak binding site; Kellogg et al., 2018), the distribution of MAP4 might be reflected by the competitive binding of MAP4 and kinesin-1 to the microtubule. A sufficient concentration of kinesin-1 might remove MAP4 from the weak binding site (Fig. 4). However, MAP4 still remains anchored at the anchor point, and the remaining detached region of MAP4 may fold and accumulate above the intertubulin–dimer groove. Thus, although MAP4 and kinesin-1 compete to bind to the weak site at the intratubulin–dimer interface, they can simultaneously bind to the microtubule after a state of equilibrium is achieved; MAP4 and kinesin-1 are bound to the interdimer and intradimer interface, respectively, in the equilibrium state (Figs. 1 and 3A). It should also be noted that as opposed to the kinesin motor binding, the binding of dynein to the microtubule was not inhibited by Tau family MAPs (Dixit et al., 2008). Tau and MAP4 structures clearly indicate that the microtubule-binding domain of dynein does not compete with the MAP4-binding site on the microtubule; our finding is consistent with the results of a previous study in which kinesin and dynein motilities were differentially regulated by Tau (Fig. S3 D; Dixit et al., 2008).

The concentrations of tubulin in living cells including cardiomyocytes were estimated to be as high as several micrometers, and the concentrations of MAP4 and kinesin-1 in cardiomyocytes were approximately one order of magnitude lower than that of tubulin (Gard and Kirschner, 1987; Mozziconacci et al., 2008; Fishilevich et al., 2016). These data suggest that in vitro protein concentrations used in these biochemical and structural studies are not far from the in vivo conditions. Thus, it is not a great surprise that the increased concentration of 5R-MAP4 in cardiomyocytes induced by mechanical stress or pressure overload reportedly interfered with the microtubule-based transport of junctophilin-2 or β-adrenergic receptor by kinesin-1 (Cheng et al., 2005; Zhang et al., 2014). Cryo-EM results of the present study provided the structural basis for kinesin inhibition by 5R-MAP4. In the 5R-MAP4–microtubule complex, MAP4

accumulation above the anchor point is much stronger than that of 4R-MAP4 (Fig. 3, A and B). The folded 5R-MAP4 density became equivalent to the kinesin-1 densities at the forward and rear sides of the anchor point, suggesting the presence of some interactions between 5R-MAP4 and microtubule-bound kinesin-1 (Fig. 4). Thus, some other mechanism may be responsible for kinesin inhibition caused by the direct binding of 5R-MAP4 to kinesin-1, for example, a decrease in or blocking of the kinesin-1 ATPase activity at some point.

Overall, our cryo-EM study provides a detailed structural view of the Tau family MAPs bound to the microtubule. It provides insight on the molecular mechanisms underlying microtubule binding, microtubule stabilization, and kinesin inhibition by MAPs, although the interaction sites between MAP4 and kinesin-1 are still not fully understood because of the flexibility or the heterogeneity of MAP4 structure. Future structural and cell biological studies are warranted to elucidate all the functions of Tau family MAPs, including the mechanism of microtubule bundling or how MAPs organize the microtubule in living cells.

Materials and methods

Protein purification

Tubulin was purified from porcine brain by six cycles of cold-induced microtubule depolymerization and warm-induced microtubule repolymerization (Yajima et al., 2012). A high-molarity Pipes buffer (1 M Pipes, pH 6.8, adjusted with KOH, 1 mM EGTA, and 1 mM $MgCl_2$) was used to remove contaminating MAPs. The bovine microtubule-binding domain fragments of MAP4, 4R-MAP4, and 5R-MAP4 were expressed in *Escherichia coli* BL21 (DE3) cells (Novagen) and purified by cation exchange chromatography (HiTrap SP HP; GE Healthcare), followed by hydrophobic chromatography (HiTrap butyl FF; GE Healthcare; Tokuraku et al., 2003). The mouse kinesin-1 (KIF5C) motor domain (residues 1–345 and a 7-His-tag) was expressed in *E. coli* BL21 (DE3) cells (Novagen) and purified by immobilized metal affinity chromatography (HisTrap; GE Healthcare) followed by cation exchange chromatography (Mono S; GE Healthcare; Morikawa et al., 2015).

Microtubule cosedimentation assay

For the simultaneous binding of kinesin-1 and MAP4, 5 µM (final concentration) tubulin was polymerized in PEM buffer (100 mM Pipes-KOH, pH 6.8, 1 mM $MgCl_2$, and 1 mM EGTA) containing 20% glycerol and 1 mM GTP at 37°C for 60 min and then stabilized by incubating with 10 µM taxol at 37°C for 5 min. The taxol-stabilized microtubules were incubated with various concentrations (0–20 µM) of kinesin-1 at 37°C for 5 min. Subsequently, various concentrations (0–16 µM) of MAP4 fragments were added and incubated at 37°C for another 5 min. Samples were centrifuged at 25,000 *g* for 15 min at 37°C using a S100AT6 rotor in an ultracentrifuge himac CS100GX II (Hitachi Koki). The separated supernatant and pellet fractions were loaded onto SDS-PAGE gels and stained with Coomassie brilliant blue R250. All samples were electrophoresed three times using different gels, and band intensities were analyzed using ImageJ (National Institutes of Health). Statistical analysis was conducted using Prism 6.0 (GraphPad Software).

Grid preparation and cryo-EM data collection

10 µM tubulin was polymerized in polymerization buffer (PEM-GTP and 7% DMSO) at 37°C for 60 min. Taxol was added in a stepwise manner to attain a final concentration of 10 µM. 10 µM 4R-MAP4 or 5R-MAP4 was subsequently added to the solution. Kinesin-1 was diluted to 10 µM in PEM buffer with 1 mM AMP-PNP. A 5-µl drop of the polymerized microtubule-MAP4 (3–10 µM) was placed onto a glow-discharged holey carbon grid (R2/2; Quantifoil). After 30 s, the solution was wicked away with a piece of Whatman no. 1 filter paper, and a 5-µl drop of kinesin-1 (10 µM) was quickly applied. After another 60 s, the grid was washed with PEM buffer containing 5 mM AMP-PNP, blotted for 5 s with blot force of 20, and then plunge-frozen into liquid ethane by using a semiautomated vitrification device (Vitrobot Mark IV; FEI) in 100% humidity at 27°C. Data acquisition was performed by using 200-kV field emission cryo-EM (Tecnai Arctica; FEI) at 78,000-fold nominal magnification with an FEI Falcon II direct detection camera under low-dose condition in the data acquisition software Serial EM (Mastronarde, 2005). All the data were collected by using Falcon Hack as a video with 34 subframes at 45 e^{-1}/pixels/s in a total electron dose of 55 $e^{-1}/Å^2$ and a pixel size of 1.28 Å/pixel. The defocus range of the dataset was set to a range of −1.5 to −2.5 µm.

Image processing and 3D reconstruction from cryo-EM images

Image processing was performed using the software MotionCorr (Li et al., 2013) and CTFFIND3 (Mindell and Grigorieff, 2003) as described previously (Yamagishi et al., 2016); images without a significant drift and astigmatism were used for further analysis. Images of a 14-protofilament microtubule complexed with MAP4 and kinesin-1 were selected and semi-automatically straightened using the "unbend" program of Ruby-Helix (Metlagel et al., 2007). Segments were extracted at a spacing of 80 Å using a box size of 768 × 768 pixels. The stack file combined by the "add to stack" command of IMOD (Kremer et al., 1996) was then applied to the seam-search scripts (Zhang and Nogales, 2015). We used EMD-6353, the kinesin that attaches to the GDP–microtubule as the 3D reference model to precisely separate α- and β-tubulin (Zhang and Nogales, 2015). The local refinement was performed twice using Frealign version 9 (Grigorieff, 2007), followed by determination of the seam position. Using refined alignment particles with the correct seam, 3D structures were reconstructed assuming either pseudohelical symmetry (HP) or no symmetry (C1). The helical parameters for three-start tubulin monomers (twist and rise) were measured using Relion helix toolbox program (Scheres, 2012) from the C1 reconstruction and applied to the next HP reconstruction. Two rounds of seam search were performed to obtain the final reconstruction. The resolution was analyzed using Fourier shell correlation. Local resolutions were estimated using ResMap program (Kucukelbir et al., 2014). A negative B-factor (−200) was applied to sharpen the final map using Bfactor program (http://grigoriefflab.janelia.org/bfactor).

Atomic model fitting and refinement

The atomic structures of kinesin-1 and α- and β-tubulins in the kinesin-1–tubulin complex model (PDB ID: 4UY0; Atherton et al., 2014) were independently fitted into the cryo-EM density map using the Fit in Map tool in UCSF Chimera (Pettersen et al., 2004).

Accession numbers

Cryo-EM maps have been deposited to the EMDB under accession codes EMD-9637 for 5R-MAP4–kinesin-1–microtubule complex and EMD-9638 for 4R-MAP4–kinesin-1–microtubule complex.

Online supplemental material

Fig. S1 shows the resolution and data collection statistics for the cryo-EM reconstructions of MAP4–kinesin-1–microtubule complex. Fig. S2 shows the local resolution estimates of the MAP4–kinesin-1–microtubule complex structures. Fig. S3 shows that dynein does not compete the microtubule binding site with MAP4.

Acknowledgments

We are grateful to G. McMullan for the help in setting up Falcon Hack to record all subframes with the Falcon2 camera, R. Zhang for instructions for analyzing the cryo-EM data, and K. Ori-Mckenney for critical reading of this manuscript.

This work was supported by Japan Society for the Promotion of Science KAKENHI (16K14704 to K. Tokuraku, 15H01656 and 17H05897 to H. Shigematsu, and 15K08168 to R. Nitta), AMED-CREST from Japan Agency for Medical Research and Development (1005341 to R. Nitta), Japan Science and Technology Agency/PRESTO (JPMJPR14L2 to T. Imasaki), Takeda Science Foundation to R. Nitta, Mochida Memorial Foundation for Medical and Pharmaceutical Research to R. Nitta, and the Uehara Memorial Foundation to R. Nitta.

The authors declare no competing financial interests.

Author contributions: R. Nitta, K. Tokuraku, and M. Shirouzu conceived the project. C. Doki, M. Aoki, and A. Sakamoto performed biochemical analyses. H. Shigematsu, T. Imasaki, T. Sumi, T. Uchikubo-Kamo, and R. Nitta performed the cryo-EM analysis. All authors discussed the results, and R. Nitta, H. Shigematsu, T. Imasaki, and K. Tokuraku wrote the manuscript.

Submitted: 29 November 2017
Revised: 2 July 2018
Accepted: 11 September 2018

References

Aizawa, H., Y. Emori, H. Murofushi, H. Kawasaki, H. Sakai, and K. Suzuki. 1990. Molecular cloning of a ubiquitously distributed microtubule-associated protein with Mr 190,000. *J. Biol. Chem.* 265:13849–13855.

Al-Bassam, J., R.S. Ozer, D. Safer, S. Halpain, and R.A. Milligan. 2002. MAP2 and tau bind longitudinally along the outer ridges of microtubule protofilaments. *J. Cell Biol.* 157:1187–1196. https://doi.org/10.1083/jcb.200201048

Atherton, J., I. Farabella, I.M. Yu, S.S. Rosenfeld, A. Houdusse, M. Topf, and C.A. Moores. 2014. Conserved mechanisms of microtubule-stimulated ADP release, ATP binding, and force generation in transport kinesins. *eLife.* 3:e03680. https://doi.org/10.7554/eLife.03680

Chau, M.F., M.J. Radeke, C. de Inés, I. Barasoain, L.A. Kohlstaedt, and S.C. Feinstein. 1998. The microtubule-associated protein tau cross-links to two distinct sites on each alpha and beta tubulin monomer via separate domains. *Biochemistry.* 37:17692–17703. https://doi.org/10.1021/bi9812118

Chen, J., Y. Kanai, N.J. Cowan, and N. Hirokawa. 1992. Projection domains of MAP2 and tau determine spacings between microtubules in dendrites and axons. *Nature.* 360:674–677. https://doi.org/10.1038/360674a0

Cheng, G., F. Qiao, T.N. Gallien, D. Kuppuswamy, and G. Cooper IV. 2005. Inhibition of beta-adrenergic receptor trafficking in adult cardiocytes by MAP4 decoration of microtubules. *Am. J. Physiol. Heart Circ. Physiol.* 288:H1193–H1202. https://doi.org/10.1152/ajpheart.00109.2004

Dehmelt, L., and S. Halpain. 2005. The MAP2/Tau family of microtubule-associated proteins. *Genome Biol.* 6:204. https://doi.org/10.1186/gb-2004-6-1-204

Dixit, R., J.L. Ross, Y.E. Goldman, and E.L. Holzbaur. 2008. Differential regulation of dynein and kinesin motor proteins by tau. *Science.* 319:1086–1089. https://doi.org/10.1126/science.1152993

Drewes, G., A. Ebneth, and E.M. Mandelkow. 1998. MAPs, MARKs and microtubule dynamics. *Trends Biochem. Sci.* 23:307–311. https://doi.org/10.1016/S0968-0004(98)01245-6

Ebneth, A., R. Godemann, K. Stamer, S. Illenberger, B. Trinczek, and E. Mandelkow. 1998. Overexpression of tau protein inhibits kinesin-dependent trafficking of vesicles, mitochondria, and endoplasmic reticulum: implications for Alzheimer's disease. *J. Cell Biol.* 143:777–794. https://doi.org/10.1083/jcb.143.3.777

Ennulat, D.J., R.K. Liem, G.A. Hashim, and M.L. Shelanski. 1989. Two separate 18-amino acid domains of tau promote the polymerization of tubulin. *J. Biol. Chem.* 264:5327–5330.

Fishilevich, S., S. Zimmerman, A. Kohn, T. Iny Stein, T. Olender, E. Kolker, M. Safran, and D. Lancet. 2016. Genic insights from integrated human proteomics in GeneCards. *Database (Oxford).* 2016:baw030. https://doi.org/10.1093/database/baw030

Fitzpatrick, A.W.P., B. Falcon, S. He, A.G. Murzin, G. Murshudov, H.J. Garringer, R.A. Crowther, B. Ghetti, M. Goedert, and S.H.W. Scheres. 2017. Cryo-EM structures of tau filaments from Alzheimer's disease. *Nature.* 547:185–190. https://doi.org/10.1038/nature23002

Gamblin, T.C., K. Nachmanoff, S. Halpain, and R.C. Williams Jr. 1996. Recombinant microtubule-associated protein 2c reduces the dynamic instability of individual microtubules. *Biochemistry.* 35:12576–12586. https://doi.org/10.1021/bi961135d

Gard, D.L., and M.W. Kirschner. 1987. Microtubule assembly in cytoplasmic extracts of Xenopus oocytes and eggs. *J. Cell Biol.* 105:2191–2201. https://doi.org/10.1083/jcb.105.5.2191

Grigorieff, N. 2007. FREALIGN: high-resolution refinement of single particle structures. *J. Struct. Biol.* 157:117–125. https://doi.org/10.1016/j.jsb.2006.05.004

Hagiwara, H., H. Yorifuji, R. Sato-Yoshitake, and N. Hirokawa. 1994. Competition between motor molecules (kinesin and cytoplasmic dynein) and fibrous microtubule-associated proteins in binding to microtubules. *J. Biol. Chem.* 269:3581–3589.

Hardy, J., K. Duff, K.G. Hardy, J. Perez-Tur, and M. Hutton. 1998. Genetic dissection of Alzheimer's disease and related dementias: amyloid and its relationship to tau. *Nat. Neurosci.* 1:355–358. https://doi.org/10.1038/1565

Hirokawa, N., Y. Shiomura, and S. Okabe. 1988. Tau proteins: the molecular structure and mode of binding on microtubules. *J. Cell Biol.* 107:1449–1459. https://doi.org/10.1083/jcb.107.4.1449

Joly, J.C., G. Flynn, and D.L. Purich. 1989. The microtubule-binding fragment of microtubule-associated protein-2: location of the protease-accessible site and identification of an assembly-promoting peptide. *J. Cell Biol.* 109:2289–2294. https://doi.org/10.1083/jcb.109.5.2289

Kar, S., J. Fan, M.J. Smith, M. Goedert, and L.A. Amos. 2003. Repeat motifs of tau bind to the insides of microtubules in the absence of taxol. *EMBO J.* 22:70–77. https://doi.org/10.1093/emboj/cdg001

Kellogg, E.H., N.M.A. Hejab, S. Poepsel, K.H. Downing, F. DiMaio, and E. Nogales. 2018. Near-atomic model of microtubule-tau interactions. *Science.* 360:1242–1246. https://doi.org/10.1126/science.aat1780

Kremer, J.R., D.N. Mastronarde, and J.R. McIntosh. 1996. Computer visualization of three-dimensional image data using IMOD. *J. Struct. Biol.* 116:71–76. https://doi.org/10.1006/jsbi.1996.0013

Kucukelbir, A., F.J. Sigworth, and H.D. Tagare. 2014. Quantifying the local resolution of cryo-EM density maps. *Nat. Methods.* 11:63–65. https://doi.org/10.1038/nmeth.2727

Li, X., P. Mooney, S. Zheng, C.R. Booth, M.B. Braunfeld, S. Gubbens, D.A. Agard, and Y. Cheng. 2013. Electron counting and beam-induced motion

correction enable near-atomic-resolution single-particle cryo-EM. *Nat. Methods.* 10:584–590. https://doi.org/10.1038/nmeth.2472

Mastronarde, D.N. 2005. Automated electron microscope tomography using robust prediction of specimen movements. *J. Struct. Biol.* 152:36–51. https://doi.org/10.1016/j.jsb.2005.07.007

Metlagel, Z., Y.S. Kikkawa, and M. Kikkawa. 2007. Ruby-Helix: an implementation of helical image processing based on object-oriented scripting language. *J. Struct. Biol.* 157:95–105. https://doi.org/10.1016/j.jsb.2006.07.015

Mindell, J.A., and N. Grigorieff. 2003. Accurate determination of local defocus and specimen tilt in electron microscopy. *J. Struct. Biol.* 142:334–347. https://doi.org/10.1016/S1047-8477(03)00069-8

Mogessie, B., D. Roth, Z. Rahil, and A. Straube. 2015. A novel isoform of MAP4 organises the paraxial microtubule array required for muscle cell differentiation. *eLife.* 4:e05697. https://doi.org/10.7554/eLife.05697

Morikawa, M., H. Yajima, R. Nitta, S. Inoue, T. Ogura, C. Sato, and N. Hirokawa. 2015. X-ray and Cryo-EM structures reveal mutual conformational changes of Kinesin and GTP-state microtubules upon binding. *EMBO J.* 34:1270–1286. https://doi.org/10.15252/embj.201490588

Mozziconacci, J., L. Sandblad, M. Wachsmuth, D. Brunner, and E. Karsenti. 2008. Tubulin dimers oligomerize before their incorporation into microtubules. *PLoS One.* 3:e3821. https://doi.org/10.1371/journal.pone.0003821

Panda, D., J.C. Samuel, M. Massie, S.C. Feinstein, and L. Wilson. 2003. Differential regulation of microtubule dynamics by three- and four-repeat tau: implications for the onset of neurodegenerative disease. *Proc. Natl. Acad. Sci. USA.* 100:9548–9553. https://doi.org/10.1073/pnas.1633508100

Pettersen, E.F., T.D. Goddard, C.C. Huang, G.S. Couch, D.M. Greenblatt, E.C. Meng, and T.E. Ferrin. 2004. UCSF Chimera—a visualization system for exploratory research and analysis. *J. Comput. Chem.* 25:1605–1612. https://doi.org/10.1002/jcc.20084

Santarella, R.A., G. Skiniotis, K.N. Goldie, P. Tittmann, H. Gross, E.M. Mandelkow, E. Mandelkow, and A. Hoenger. 2004. Surface-decoration of microtubules by human tau. *J. Mol. Biol.* 339:539–553. https://doi.org/10.1016/j.jmb.2004.04.008

Scheres, S.H. 2012. RELION: implementation of a Bayesian approach to cryo-EM structure determination. *J. Struct. Biol.* 180:519–530. https://doi.org/10.1016/j.jsb.2012.09.006

Schweers, O., E. Schönbrunn-Hanebeck, A. Marx, and E. Mandelkow. 1994. Structural studies of tau protein and Alzheimer paired helical filaments show no evidence for beta-structure. *J. Biol. Chem.* 269:24290–24297.

Seitz, A., H. Kojima, K. Oiwa, E.M. Mandelkow, Y.H. Song, and E. Mandelkow. 2002. Single-molecule investigation of the interference between kinesin, tau and MAP2c. *EMBO J.* 21:4896–4905. https://doi.org/10.1093/emboj/cdf503

Spillantini, M.G., and M. Goedert. 1998. Tau protein pathology in neurodegenerative diseases. *Trends Neurosci.* 21:428–433. https://doi.org/10.1016/S0166-2236(98)01337-X

Tokuraku, K., K. Matsushima, T. Matui, H. Nakagawa, M. Katsuki, R. Majima, and S. Kotani. 2003. The number of repeat sequences in microtubule-associated protein 4 affects the microtubule surface properties. *J. Biol. Chem.* 278:29609–29618. https://doi.org/10.1074/jbc.M302186200

Tokuraku, K., T.Q. Noguchi, M. Nishie, K. Matsushima, and S. Kotani. 2007. An isoform of microtubule-associated protein 4 inhibits kinesin-driven microtubule gliding. *J. Biochem.* 141:585–591. https://doi.org/10.1093/jb/mvm063

Trinczek, B., A. Ebneth, E.M. Mandelkow, and E. Mandelkow. 1999. Tau regulates the attachment/detachment but not the speed of motors in microtubule-dependent transport of single vesicles and organelles. *J. Cell Sci.* 112:2355–2367.

Yajima, H., T. Ogura, R. Nitta, Y. Okada, C. Sato, and N. Hirokawa. 2012. Conformational changes in tubulin in GMPCPP and GDP-taxol microtubules observed by cryoelectron microscopy. *J. Cell Biol.* 198:315–322. https://doi.org/10.1083/jcb.201201161

Yamagishi, M., H. Shigematsu, T. Yokoyama, M. Kikkawa, M. Sugawa, M. Aoki, M. Shirouzu, J. Yajima, and R. Nitta. 2016. Structural Basis of Backwards Motion in Kinesin-1-Kinesin-14 Chimera: Implication for Kinesin-14 Motility. *Structure.* 24:1322–1334. https://doi.org/10.1016/j.str.2016.05.021

Zhang, R., and E. Nogales. 2015. A new protocol to accurately determine microtubule lattice seam location. *J. Struct. Biol.* 192:245–254. https://doi.org/10.1016/j.jsb.2015.09.015

Zhang, C., B. Chen, A. Guo, Y. Zhu, J.D. Miller, S. Gao, C. Yuan, W. Kutschke, K. Zimmerman, R.M. Weiss, et al. 2014. Microtubule-mediated defects in junctophilin-2 trafficking contribute to myocyte transverse-tubule remodeling and Ca2+ handling dysfunction in heart failure. *Circulation.* 129:1742–1750. https://doi.org/10.1161/CIRCULATIONAHA.113.008452